A time-dependent ice accretion model for trap-setting fishing vessels with filigree structures

Thomas DeNucci[1,*], Daniel Brahan[2], Peter McGonagle[1], Colman Schofield[1] and Delaney Taplin-Patterson[1]

ABSTRACT

This paper describes a time-dependent methodology for calculating the rate of ice accretion on vessels with filigree structures. It combines Newton's Second Law for spray droplet trajectories with time varying flow velocities determined using computational fluid dynamics (CFD). The mass flux of ice is determined by solving a set of partial differential equations describing the conservation of mass, heat, and salt in the boundary layer of brine near the ice surface. Icing predictions numerically generated by this approach are evaluated against current stability regulations for fishing vessels.

KEY WORDS

Ice Accretion; Safety; Stability; Fishing Vessels; Porous Surface

INTRODUCTION

The fishing vessel *Scandies Rose* capsized off the coast of Alaska, USA, in heavy spray-icing conditions on December 31, 2019, with five of the seven onboard perishing. A Marine Board of Investigation conducted by the U.S. Coast Guard and the National Transportation Safety Board (NTSB) identified inaccurate accounting of ice on deck gear, specifically fishing pots, as a causal factor, National Transportation Safety Board (2021).

This tragedy follows in the wake of another capsize event. In 2017, the fishing vessel *Destination* sank off St. George Island, Alaska, under heavy spray icing conditions with the loss of all six crew members onboard. Figure 1 shows icing on *Sandra Five*, a vessel operating in the same vicinity as *Destination* during the fatal storm.

Since *Scandies Rose* and *Destination* were operating on domestic voyages, they were subject to the stability standards identified in US 46 CFR Part 28 Subpart E instead of those prescribed by international regulation and survey requirements of Safety of Life at Sea (SOLAS) set forth by the International Maritime Organization (IMO). However, the maximum assumed icing quantities on fishing vessels are identical between these two codes – 30 $\frac{kg}{m^2}$ of ice on horizontal surfaces and 15 $\frac{kg}{m^2}$ on vertical surfaces.

[1] U.S. Coast Guard Academy, Department of Naval Architecture & Marine Engineering, New London, CT, USA)
[2] U.S. Coast Guard Academy, Department of Naval Architecture & Marine Engineering, New London, CT, USA) ORCID: 0009-0000-9997-5366
[*] Corresponding Author: thomas.w.denucci@uscga.edu

Figure 1: Ice accumulation on *Sandra Five*, National Transportation Safety Board (2017).

There are limitations to these rule-sets. First, both regulatory schemes assume uniform ice loading and do not consider the effects of list due to off-center weight additions. Uniform ice loading in storm conditions is a rare occurrence because fishing vessels rarely have wind and seas directly off their bows. Second, these rule-sets assume that icing is applied over the top and sides of the fishing pots, commonly referred to as the "shoebox method." However, crab pots are porous, being constructed of steel tubing with netting, which enables ice to accumulate in the interior of the crab pot stack.

The goal of this paper is to develop an icing model that specifically considers both the time-varying effects of icing on fishing pots and the nature of ice formation on filigree structures themselves. Knowing how, where and the rate of ice accretion will provide opportunities to develop fishing vessel designs less prone to icing. This work forms the foundational knowledge required before changes to regulations may be proposed. The results have the potential to change the modeled icing quantity and location for naval architects performing stability analysis on fishing vessels subsequently improving safety conditions for mariners onboard while protecting the marine environment.

BACKGROUND

The effects of marine icing on vessels at sea can be catastrophic. Ryerson (2009) cites hazards including a reduction in stability, damage to vessel structure, damage to equipment including winches, cranes, and antennas and slipping hazards on decks, ladders, and handrails. In the worst case, rapidly accumulating ice can cause a rise in the vessel centre of gravity which can result in a reduction of the righting arm and possible vessel capsize.

Scandies Rose and other trap-set fishing vessels are distinctive because their deck load ices differently than solid plates and cylinders because they are porous. Ice can accumulate not only on exterior surfaces, but also inside the fish pot itself, filling up space normally assumed to be empty voids on deck, National Transportation Safety Board (2021).

Table 1: *Scandies Rose* on-scene weather conditions reported by rescue team and survivors, National Transportation Safety Board (2021).

Weather Element	Value
Wind Velocity	$18 - 25$ m/s ($35 - 50$ kts)
Wind Direction (Relative to the Vessel)	045°
Significant Wave Height	$6 - 10$ m
Wave Period	$9 - 10$ sec
Water Temperature	3^oC
Air Temperature	-12^oC

All too often, all hands are lost on vessels that capsize in the Bering Sea. However, weather conditions on the night of *Scandies Rose* capsize, shown in Table 1, have been corroborated by the may-day call, survivor testimony and on-scene reports from the rescue helicopter and offer unique insight into the on-scene conditions. This paper applies these weather data and the knowledge gained from survivor testimony to the ice accretion approach outlined next.

APPROACH

Figure 2 highlights the key elements of the presented approach. The model assumes that a thin layer of ice already exists on all surfaces. The velocity flow across the vessel and crab pots are solved using CFD. The flow field is important because it influences both droplet trajectory and heat convection coefficients. However, as ice accumulates on the crab pot netting, the crab pot geometry and flow field change DeNucci et al. (2023). To account for this, the flow field is recalculated after every 30 minutes of simulation.
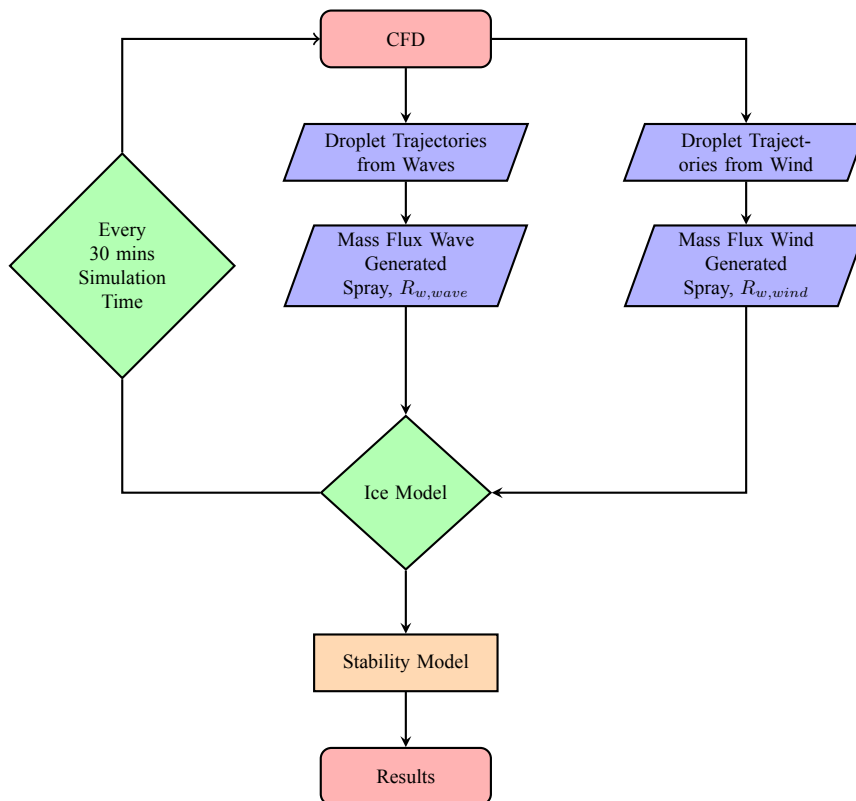

Figure 2: Flow chart of ice accretion analysis on porous surfaces.

Using the environmental conditions described in Table 1, the mass flux of spray striking the vessel is calculated. A thermodynamic heat balance between the mass and salinity of brine is solved to determine the rate of ice accretion. After 30 minutes, the crab pot porosities, flow field, mass flux and heat convection coefficient are recalculated and the rate of ice accretion is again solved using the updated data.

After the simulation finishes, the impact of ice on overall vessel stability is analysed using General Hydrostatics Software (GHS). Stability is evaluated using the wind magnitude and direction reported on the night of the capsize. Details of this approach follow.

TIME VARYING VELOCITY FLOW FIELDS

One challenge with filigree structures, crab pots on fishing vessels, are their nature of icing. As ice accumulates on the netting structure, the pot porosity changes, which results in new geometry, and subsequently, different velocity flow across the pot structure. These changes have an important effect on ice accretion and have not been accounted for in previous icing models.

Darcy-Forchheimer Law

Computational fluid dynamics is used to determine velocity flow across the crab pots. To achieve this, the pots are modelled as porous surfaces using the Darcy-Forchheimer law so that the permeability and drag coefficient of the pot structure can be determined. The Darcy-Forchheimer law serves as an augmented version of Darcy's law, which characterizes the flow of fluids through porous media. Unlike Darcy's law, the Darcy-Forchheimer equation accommodates non-linear effects observed at elevated flow velocities within porous media, offering a more comprehensive understanding of fluid dynamics at higher flow speeds.

The law, shown in equation 1, is comprised of a linear and quadratic term. At low Reynolds numbers, the pressure loss is directly proportional (linear) to the flow velocity. At higher Reynolds numbers, the pressure losses across the medium increase rapidly and become a quadratic function of velocity.

$$\Delta P = -(\frac{\beta}{\alpha}\mu\overrightarrow{V} + \frac{\beta^2}{\sqrt{\alpha}}\rho C_d|\overrightarrow{V}|\overrightarrow{V})\delta \tag{1}$$

where

C_d = quadratic drag coefficient ($\frac{1}{m}$)

ΔP = change in pressure (Pa)

$\overrightarrow{V}$ = velocity magnitude ($\frac{m}{s}$)

α = permeability (m^2)

β = porosity

δ = the thickness of medium (m)

μ = dynamic viscosity (Pa s)

ρ = density ($\frac{kg}{m^3}$)

To solve for permeability and drag coefficient, the pressure drop across a singular crab pot of specific porosity is measured for various wind velocities (0 to 40 knots). The net orientation and webbing thickness of the crab pot match those loaded on *Scandies Rose*. After varying the wind speed across the pot, the pot porosity is changed and the pressure drop is measured again at the new porosity. Changes in porosity, illustrated in Figure 3, are achieved by changing the web thickness to achieve the desired porosity value (80% - 10%). Results are shown in Table 2.

Using the Darcy-Forchheimer Law, a second-order polynomial is fit to the data describing the pressure drop and wind velocity at each crab pot porosity. The coefficients of this polynomial curve describe the crab pot permeability (m^2), a linear term, and quadratic drag-coefficient (m^{-1}), a quadratic term. Results are shown in Table 3.
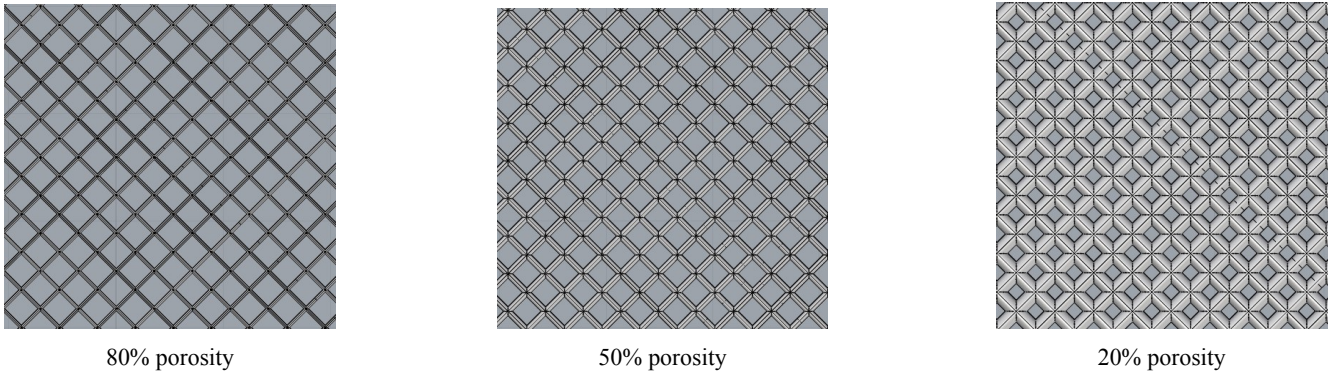
80% porosity   50% porosity   20% porosity

Figure 3: Crab pot netting at various porosities.

Table 2: Change in pressure across crab Pot netting at different wind velocities [Pa]

Wind Velocity		Crab Pot Porosity (γ, %)							
(knots)	(m/s)	80	70	60	50	40	30	20	10
0	0	0	0	0	0	0	0	0	0
2.5	1.29	0.22	0.27	0.35	0.48	0.50	0.63	0.69	0.82
5	2.57	0.86	1.05	1.33	1.64	1.98	2.49	2.88	3.26
10	5.14	3.37	4.15	5.30	6.54	7.99	10.01	11.59	13.05
15	7.72	7.52	9.335	11.89	14.69	17.97	22.56	26.14	29.38
20	10.29	13.39	16.25	21.09	25.91	31.93	40.14	46.45	52.26
25	12.86	20.96	25.78	32.90	40.75	49.95	62.3	74.5	81.54
30	15.43	30.13	37.08	47.33	58.66	71.8	90.57	104.5	117.5
40	20.58	53.6	65.89	84.17	100.15	127.55	158.20	184.7	208.8

Using values in Table 3, the crab pot stack can then be modelled as a porous surface and the velocity field is again determined using CFD. Local icing quantities (kg/m^2) are directly related to porosity by assuming the ice accumulates on the crab pot webbing in a half-cylindrical fashion. This is discussed later in the paper.

SEA SPRAY FLUX, R_w

Sea spray flux is the precursor to ice formulation and is required to accurately predict the rate of ice accretion on the vessel. Spray originates from both wind-wave and vessel-wave interactions, although the majority of the sea spray striking the vessel comes from vessel-wave interactions. Wind-generated sea spray is caused by lifting droplets from wave crests on the ocean surface. Wind-spray is a small, but constant water flux present in the air when the wind speed is greater than nine metres per second. Deterministic methods to calculate wind-generated spray flux are found in Jones and Andreas (2012). Wave-generated sea spray is caused by the collision of waves with the vessel. Wave-generated sea spray is generally the source of large but brief periodic water flux that originates near the bow of the vessel Hansen (2012). Zakrzewski (1986) and Lozowski et al. (2000) provide methods to calculate this flux. Sea spray flux calculations specific to *Scandies Rose* can be referenced in Brahan et al. (2023).

Using Newton's Second Law for droplet motion, individual water droplets were injected into the velocity flow field and tracked throughout their flight to determine if they intersect the vessel. Since it is impractical to simulate every droplet of water generated by sea spray, droplets are re-characterized as "parcels" of the mass flux Brahan et al. (2023). Jones and Andreas (2012) determined the size and quantity of droplets at a given height above a free surface for given wind speeds. Since the total water mass present in a cubic meter of air can be calculated, a relationship between percent contribution of

Table 3: Permeability and drag coefficient values for crab pots as a function of porosity.

Porosity	Permeability (α)	Drag Coefficient (C_d)
80	1.02E-02	1.59E-02
70	4.82E-03	1.77E-02
60	1.32E-03	1.61E-02
50	1.07E-04	9.96E-03
40	6.82E-04	3.64E-02
30	4.96E-05	2.14E-02
20	1.95E-05	3.78E-02
10	2.43E-04	6.16E-01

mass for a given droplet size was established Brahan et al. (2023). An analogous correlation was developed by Ryerson (1995), who measured the droplet number concentration and droplet size distribution of a wave-spray cloud using a strobo-scopic camera on the U.S. Coast Guard Cutter *Midgett* in the Bering Sea.

Since wave-generated spray only occurs when encountering a wave and for the duration of the wave encounter, the wave-generated flux behaves like a step function. When the vessel encounters a wave, wave flux comes into the system; it is zero at all other times Brahan et al. (2023).

ICING MODEL

A system of partial differential equations governs the ice and brine flux. The ice flux depends on several factors including the incoming latent heat of mass from the ocean, heat flux, brine flux, and brine salinity. The set of differential equations which follow are analyzed as a series of nodes on the side of the crab pot stack. These are numerically solved for each time step at each node using the method of lines DeNucci et al. (2023).

Wet Icing

Normally, marine icing occurs in a wet state. This occurs when atmospheric conditions are conducive to freezing, but only part of the incoming spray flux freezes. The remaining spray flows off the surface as brine. Modelling the crab pot net as series of nodes, each node receives water from the free surface and brine flux. Conservation of mass, heat and salt give the approximate differential equations of the brine film, Horjen (1990); DeNucci et al. (2023):

$$\frac{\delta X}{\delta t} + \nabla_t(v_b X) = R_w - I \tag{2}$$

$$c_b X (\frac{\delta}{\delta t} + v_b \nabla_t) T_b = Q + (1 - \sigma) l_f I \tag{3}$$

$$\frac{X}{S_b}(\frac{\delta}{\delta t} + v_b \nabla_t) S_b = I(1 - \sigma) - R_w(1 - \frac{S_w}{S_b}) \tag{4}$$

where X is the local brine amount per unit area ($\frac{kg}{m^2}$), T_b is the brine temperature and S_b the brine salinity (in parts per thousand). R_w is the impinging sea spray flux ($\frac{kg}{m^2 s}$) and I ($\frac{kg}{m^2 s}$) is the rate of accretion of both the ice and the brine trapped in the ice. The variable v_b is the brine velocity and ∇_t is the differential operator in the tangential direction, i.e., along the direction in which the brine will move. c_b is the specific heat capacity of the brine, σ is the fraction of entrapped brine in

the accretion, l_f is the latent heat of freezing and S_w is the salinity of seawater. Mass flux due to evaporation is neglected.

Dry Icing

If the sea spray flux is relatively low, and the weather is sufficiently cold, it is possible for all the incoming spray to freeze on impact, Hansen (2012). This condition, referred to as dry icing, occurs when the heat transport away from the brine is greater than or equal to the latent heat produced if all the impinging spray freezes. The initial assumption was that only wet icing occurred on the vessel. However, initial simulations revealed that certain portions of the crab pot stack do not receive heavy quantities of mass flux into the system. Furthermore, the cyclical nature of heavy then light mass flux due to vessel-wave interaction causes different locations on the crab pot stack to freeze differently.

These factors combine to create a cycle of wet and dry icing, where dry icing often occurs between the wave-generated sea spray events. Initial simulations showed that wet and dry icing occurred concurrently on different nodes and at the same node for different instances of time, DeNucci et al. (2023). This phenomenon impacts the rate of ice accretion because residual brine flux may still be present at a given node location as the process of icing repeats itself. One important result of this phenomenon, shown in equation 5, is the modification of established icing equations to include the impact of brine on the different icing modes DeNucci et al. (2023).

$$R_w + X \leq \frac{Q}{l_f(1 - \sigma)}$$ (5)

where R_w is the spray flux during a spray event and σ is the interfacial coefficient, assumed to be 0.34. X is the local brine amount per unit area ($\frac{kg}{m^2}$) and l_f is the latent heat of freezing.

Heat Balance

The icing model requires a thermodynamic heat balance governed by a set of differential equations Horjen (1990). When water droplets strike a vessel, they freeze due to various heat fluxes. The heat fluxes are convective heat flux (Q_c), evaporative heat flux (Q_e), radiant heat flux (Q_r), and the heat capacity of impinging water droplets (Q_d). The heat flux due to viscous aerodynamic heating (Q_v), conduction (Q_a), and kinetic energy of in-coming droplets (Q_a) are usually neglected because they are small. The icing model uses a parameterized form in which heat flux equations are presented as functions of T_s, where T_s is the equilibrium freezing temperature of the surface brine.

The convective heat flux is the sensible heat flux between the freezing surface and the surrounding air and is given by equation 6.

$$Q_c = h_c(T_s - T_a)$$ (6)

where h_c is the heat transfer coefficient, where T_s the temperature of the water at the air-water interface, and T_a the air temperature.

The heat transfer coefficient is given by equation 7:

$$h_c = \frac{Nuk_a}{L}$$ (7)

where k_a is the thermal conductivity of air and L is the characteristic length of the component, which for cylindrical com-

ponents is the diameter. Nu is the is the Nusselt number defined for cylindrical components.

Q_e, the evaporative heat loss to the surrounding air flow is given as equation 8.

$$Q_e = h_c (\frac{Pr}{Sc})^{0.63} \frac{\epsilon l_f}{P_{c_a}} (e_s(T_S) - RH e_a(T_a))$$ (8)

where h_c is the heat transfer coefficient, Pr is the Prandtl number, Sc is the Schmidt number, ϵ is the ratio of molecular weights of water vapor and dry air, P is the atmospheric pressure, l_v is the latent heat of vaporization for water at the surface temperature, c_a is the specific heat capacity of dry air at constant pressure, RH is the relative humidity of the air, and $e_s(T)$ is the saturated water pressure.

Q_r, the radiative heat flux is given by equation 9.

$$Q_r = \sigma(\epsilon_s T_s^4 - \epsilon_a T_a^4)$$ (9)

where ϵ is the Stefan Boltzmann constant, and ϵ_s and ϵ_a are the emissivity of the air flow and icing surface, both considered to be 1.

Q_d, the heat capacity of impinging water droplets, is presented as equation 10, Zarling (1980).

$$Q_d = R_w c_w (T_s - T_d)$$ (10)

where c_w is the specific heat capacity of water, T_d the droplet temperature of the wave spray prior to impingement, and R_w the total mass flux of water. Although the droplet temperature, T_d, can be calculated on the individual droplet scale using a method proposed by Kato (2012), a simplified assumption proposed by Stallabrass (1980) is used. The total heat out of the system, Q, is the summation of the individual heat fluxes.

Using relationships between brine salinity and brine temperature by Assur (1958) and Horjen and Vefensmo (1987), equations 3 and 4 are combined to determine the ice accretion rate:

$$I = \frac{(1 - \frac{S_w}{S_b}) R_w \frac{F(S_b)}{l_f} Q}{(1 - \sigma)(1 + F(S_b))}$$ (11)

CALCULATING RELATIONSHIP BETWEEN ICE ACCRETION AND POROSITY

Across the fishing industry, there is a high degree of variation in the size of pots vessels carry due to the many species, regions, and state or federal regulations they may operate under. Accordingly, the approach should not be bound by any set dimensions. Therefore, a general geometric relation between ice accretion and porosity was created to accommodate the majority of pot types and configurations with little to no change between each simulation.

Assuming the crab pot netting is flat, continuous, and at a 45° bias across the entire face presented towards the oncoming spray, it is possible to subdivide the large net into individual squares show in Figure 4. This approach allows full simulation of icing event given only two dimensions, R, the thickness of webbing material in the net, and L, the distance between intersections in the net.

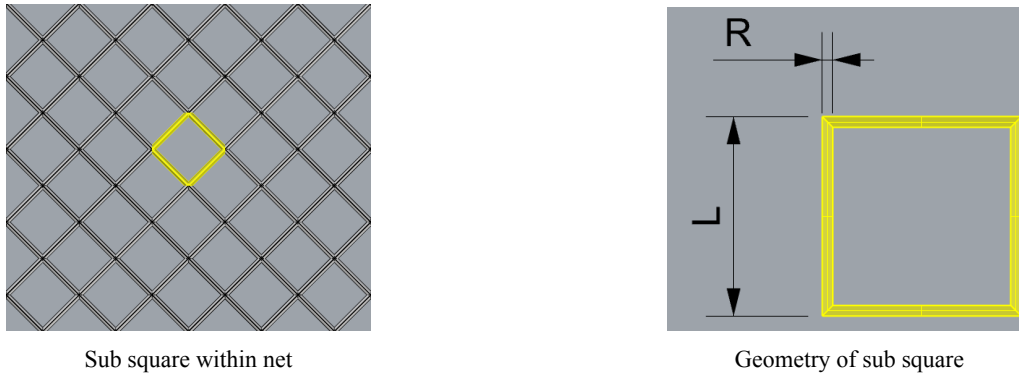Sub square within net   Geometry of sub square

Figure 4: Location and geometry of a sub-square in the net structure.

Initially, we assumed that ice would form in a cylindrical manner around each line in the netting. However, this reflects the behavior of *snow* accretion on power lines, which, given their ubiquity around the world, are well documented and researched.
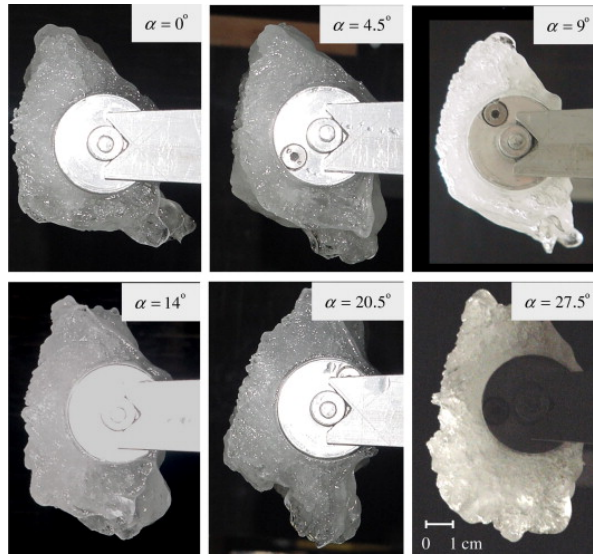

Figure 5: Profiles of ice accretions for various values of angle from horizontal, α, around stream wise axis under freezing rain conditions, Kollár and Farzaneh (2010).

Admirat (2008) notes that the *cylindrical accretion mechanism* seen on power lines is dependent on their ability to rotate due to the low torsional resistance seen by the long wires. While this rotational ability seen in the netting of crab pots, it is the accumulation of ice rather than snow drastically affects the resulting shape, making the initial cylindrical model inadequate.

Kollár and Farzaneh (2010) demonstrate that icing events on shorter, fixed, cylindrical objects, while certainly not uniform, appear much closer to a semi circle as seen in Figure 5. To better reflect this new *semi-cylindrical icing accretion mechanic*, equation 12 shows that the amount of mass due to icing is such that only half of the line would be covered in ice, thereby doubling the amount of radius (R) "consumed" per kg of ice accumulated (m_{Ice}).

$$m_{Ice} = \frac{\rho\pi}{2}\left[L(R^2 - r^2) - \frac{4}{3}R^3 + \frac{4}{3}r^3\right] \tag{12}$$

where

m_{Ice} = mass of ice accumulated per sub square (kg)

L = side length of net sub square (m)

ρ = density of ice ($\frac{kg}{m^3}$)

R = overall radius of line and accumulated ice (m)

r = initial radius of line (m)

γ = porosity of netting (%)

Equation 13 shows the relationship between icing volume and porosity. Given R, L and r, crab pot porosity is determined from the weight of ice onboard the vessel. This information is then fed back into the CFD solver, droplet trajectory and icing models to change droplet trajectory, mass flux of water into the side of the crab pot, and convection coefficients in the icing model.

$$\gamma = \frac{4r(L - R)}{L^2} \tag{13}$$

MODEL IMPROVEMENTS

One significant improvement in this approach is the incorporation of a feedback loop. Previous simulations only considered constant crab pot porosity. To implement the time varying nature of porosities in crab pots as they ice, the CFD model was updated to allow varying porosity values.

The previous model had five tiers of crab pot stacks with uniform porosity within each layer of the crab pot stack. Early simulations showed that porosity varied only in the forward third of the stack, DeNucci et al. (2023). Additionally, icing was non-uniform, meaning certain areas saw ice form at a rapid pace and indicated that the original model was not representative of the location or rate of ice accumulation. An updated model, shown in Figure 6, subdivides the crab pots into 14 clusters to more accurately capture the localized areas where porosity varies the most. Since ice rapidly accumulates on the forward starboard side of the vessel, eight smaller clusters are modelled in that location.
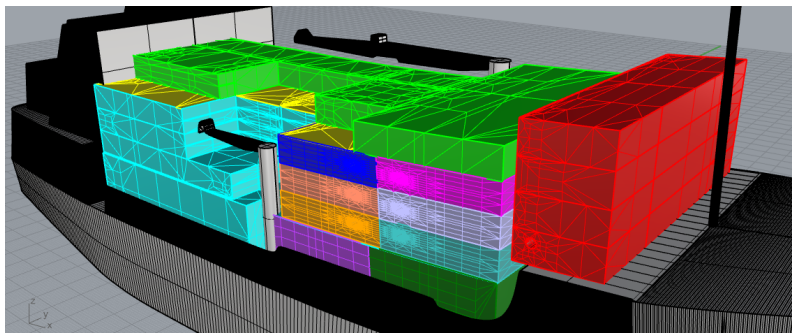

Figure 6: *Scandies Rose* CFD model. The different colored regions represent areas where porosity can be individually defined.

The CFD solver and the icing model were run at 30 minute intervals. The 30 minute interval balanced computational time with obtaining an accurate model of the phenomenon. After each interval, the porosities of the crab pots would be updated

based on the amount and extent of icing that occurred. The total simulation time was four hours, mirroring the total time icing occurred on *Scandies Rose*. Initial porosity was set to 90% throughout the crab pot stack and then reassessed for the 14 subdivided regions after every 30 minutes of simulation time.

RESULTS

Figure 7 shows the simulation results from the model presented in this paper. Ice accretes in a non-linear fashion, both in total mass accumulated and vcg of the ice on the crab pot stack. Previous simulations with 90.5% porosity (constant), shown in Figure 8, did not show any appreciable change in icing distribution.

The results showed the that vertical center of gravity (vcg) of the ice in the crab pot stack rises, as does the rate of ice accretion on the crab pot stack. This is an important point. If constant porosity is assumed throughout the simulation, the vcg remains constant and therefore underestimates the stability impact of added weight.
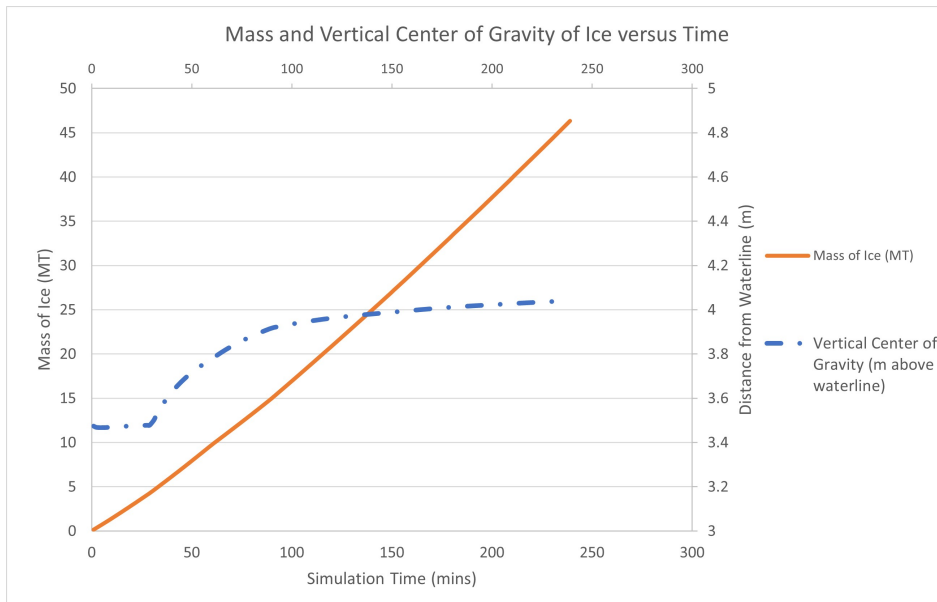

Figure 7: Mass versus vcg of ice versus time for the simulation length.

Figure 9 shows ice progression as it begins to accumulate in the upper forward region of the crab pot stack. Note, the icing scales are different between the two images. Simulation results highlight the need for a time-dependent model in order to more accurately simulate the phenomenon of icing on porous surfaces.

Stability Analysis

After obtaining ice data (mass and vcg) from the icing simulation, vessel stability was analyzed using GHS software. Figure 10 shows the hydrostatic righting curves from the icing simulation compared to the regulatory icing requirements in US 46 CFR 28.550 and International Code on Intact Stability (IS Code) 6.3 using the "shoebox" method DeNucci and Brahan (2022). The regulations required the addition of 19.89 MT of ice on the centerline of the vessel. The righting arm curve for this condition is shown as the dashed line in Figure 10.

The simulated results most nearly match the regulatory icing after a half hour of simulation time with *only* 4.26 MT (vs. 19.89 MT) of ice added to the vessel. It is important to note that the resultant ice from the simulation only accounts for ice
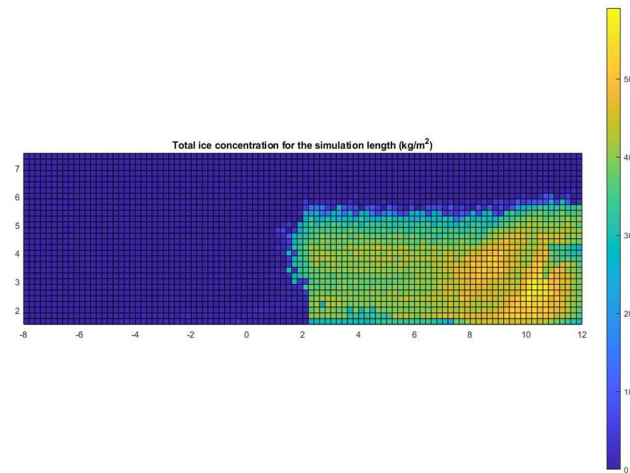
Figure 8: Ice mass per unit area (kg/m^2) for a one hour simulation with constant porosity (no feedback loop implemented). Figure displays ice accumulation for outboard starboard side of pot stack on main working deck. Origin - point (0,0) - is located at amidship and based at waterline.
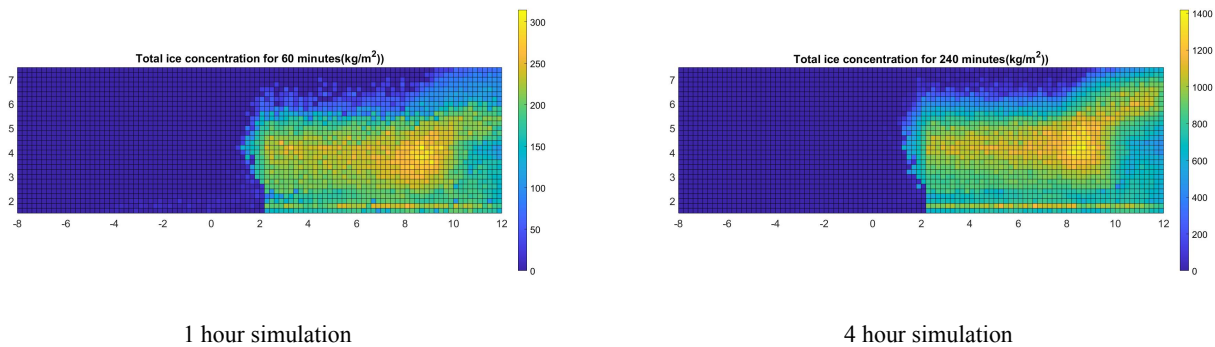

1 hour simulation   4 hour simulation

Figure 9: Ice mass per unit area (kg/m^2) at discrete times in the simulation. Crab pot porosity values are updated every 30 minutes.

on the *outer edge* of the crab pots, whereas the regulatory icing applies ice across the entire surface area of the vessel. Simulated icing also occurs farther forward on the vessel than assumed by regulation, as the centroid of ice is forward of amidships. This creates an increased righting arm at higher angles due to the large buoyant volume in the forward location of the vessel. This assumes the forward volume in the hull is watertight throughout all angles analyzed and did not take into account downflooding points.

The icing model also induces a list from off-center ice loading. Regulations require ice to be loaded uniformly centerline, whereas this icing model puts the ice loading on the outer edge of the crab pot stack. The righting arms show an induced list of almost 3° after one hour and 5° after an hour and a half. Additionally, the hour and a half case shows a lolling condition possible - an indicator the vessel is in dire circumstances. This lolling condition is a result of less ice onboard than what is applied by regulation (approximately 15 MT versus 20 MT) DeNucci and Brahan (2022). Given the extreme environment which induces these icing conditions, the righting area may not be enough to absorb the dynamic effect of wind and waves on the vessel.

Initially, *Scandies Rose* experienced wind off the starboard bow. Applying this wind as a restoring moment created an almost-imperceptible change to the righting arm and angle of list.

This analysis highlights the importance of modeling ice accretion in an off-center fashion. A comparison of righting arms
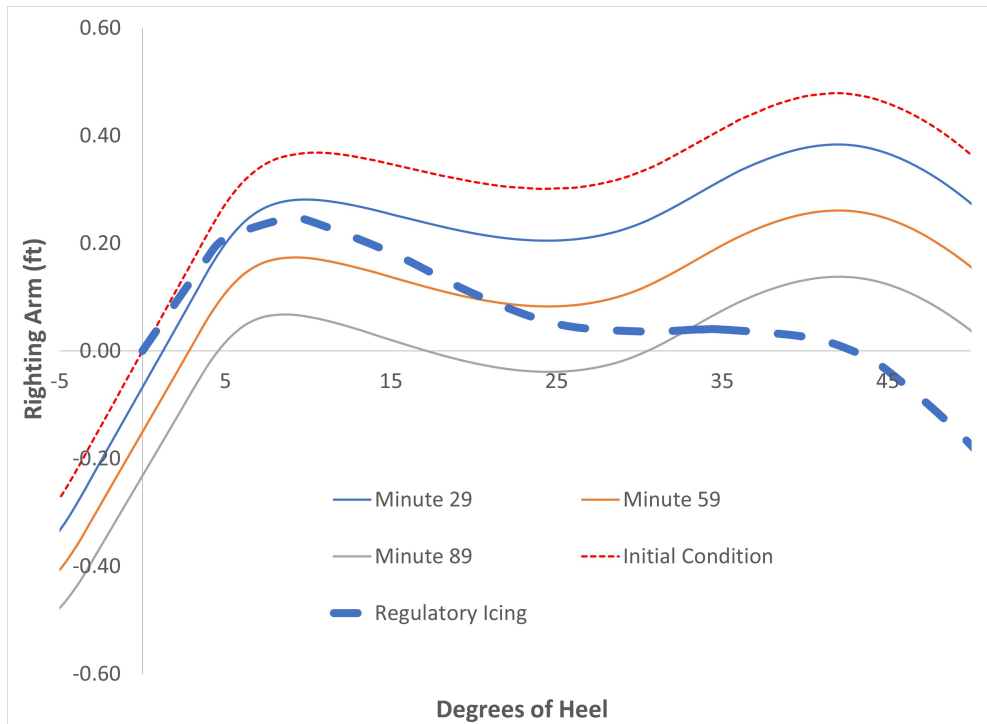
Figure 10: Static Righting Arm of *Scandies Rose* for the icing simulation. Regulatory icing, 46 CFR 28.550, is shown in the bold dashed line. Of note, downflooding points were not taken into account. Ice loads from the longer simulations capsized the vessel.

using regulatory icing requirements and the results after 89 minutes show the stark difference in a vessel's ability to withstand external forces.

CONCLUSIONS

With this model, a more accurate depiction of crab pot icing is captured. Implementing a feedback loop in the vessel icing model, while concurrently updating the pot porosities as they ice, showed both an increased rate of icing and a rise in the center of gravity of the ice over time. The accumulating ice:

1. changes the flow field, causing subsequent droplets to land in higher regions than previous simulations showed, and

2. decreases crab pot porosity, thereby increasing the sea spray flux into the system.

If permitted to continue, the center of gravity of ice will continue to rise, thereby increasing the vessel's overall center of gravity.

Off-center weight, which negatively impacts the vessel's stability, can ultimately cause vessel capsize. The effect of off-center ice is clear: less ice than required by regulation modeled in an off-center fashion puts the vessel in a worse situation than witnessed in with regulations. This paper presents an accurate, time-dependent study of how quickly ice can accumulate on the outer surface of the crab pot stack. The goal of future regulation should be to provide reasonable amount of time for the crew to intervene to prevent catastrophic capsizing.

FUTURE WORK

This study presents an ice accretion model that improves the quantitative understanding of icing phenomena on filigree structures. It only considered the outer edge of the crab pot stack and does not take into account all the intermediate surfaces where ice can accumulate. Future work should aim to quantify the ice accumulation on the interior surfaces and equipment (coiled line and buoys) of each crab pot.

While modeling the events leading up to *Scandies Rose's* capsize was one aim of this research, another is to prevent these occurrences in the future. This might be accomplished by updated stability regulations, but it is also of interest to reduce the amount of icing on the structure in the first place.

To match the net orientation on *Scandies Rose*, crab pot netting was arranged at a 45° bias to the structure of the crab pot. As a result, the brine flows in both the x- and z- directions along the webbing. Modeling the nets in the vertical direction might reduce ice accumulation because the amount of time the brine is exposed to the high convection coefficients may decrease. Other areas of interest are the effects of spray rails and the addition of flare to the hull design. All three design changes have the potential to impact the quantity of ice accumulation on a vessel in extreme weather conditions such as those *Scandies Rose* and *Destination* were subject.

CONTRIBUTION STATEMENT

Thomas DeNucci: Conceptualization; porous surface methodology; computational fluid dynamics modelling; writing – original draft. **Dan Brahan:** Methodology; droplet and ice accretion modelling; stability calculations; writing – original draft. **Peter McGonagle** Methodology; ice accretion modelling; writing - review and editing. **Colman Schofield:** Computational fluid dynamics vessel model; porosity calculations; writing - review and editing. **Delany Taplin-Patterson:** Computational fluid dynamics vessel model; porosity calculations; writing - review and editing.

REFERENCES

Admirat, P. (2008). *Wet Snow Accretion on Overhead Lines*, pages 119–169. Springer Netherlands, Dordrecht.

Assur, A. (1958). Composition of sea ice and tensile strength, arctic sea ice. *US National Academy of Science, National Research Council Publication 508*.

Brahan, D., DeNucci, T., and Glivar, G. (2023). Numerical simulation of sea spray events in extreme weather conditions. 22nd *International Conference on Computer Applications and Information Technology in the Maritime Industries*.

DeNucci, T. and Brahan, D. (2022). A digital twin for the formulation of ice accretion on vessels. 21st *International Conference on Computer Applications and Information Technology in the Maritime Industries*.

DeNucci, T., Brahan, D., Kerst, A., and Oyola, O. (2023). Improving ship safety with a digital twin for ice accretion. 22nd *International Conference on Computer Applications and Information Technology in the Maritime Industries*.

Hansen, E. (2012). *Numerical modelling of marine icing on offshore structures and vessels*. PhD thesis, Norwegian University of Science and Technology.

Horjen, I. (1990). *Numerical modelling of time-dependent marine icing, anti-icing and de-icing*. PhD thesis, Norwegian University of Science and Technology.

Horjen, I. and Vefensmo, S. (1987). Time dependent sea spray icing on ships and drill rigs - a thoeretical analysis. *Offshore Icing - Phase IV, NHL Report STF60 F87130*.

Jones, K. and Andreas, E. (2012). Sea spray concentrations and the icing of fixed offshore sea structures. *Quarterly J. Royal Meteorological Society*, 138:131–144.

Kato, R. (2012). *Modelling of ship superstructure icing: Application to ice bridge simulators*. PhD thesis, Norwegian University of Science and Technology.

Kollár, L. E. and Farzaneh, M. (2010). Wind-tunnel investigation of icing of an inclined cylinder. *International Journal of Heat and Mass Transfer*, 53(5):849–861.

Lozowski, E., Szilder, K., and Makkonen, L. (2000). Computer simulation of marine ice accretion. *Philosophical Transactions: Mathematical, Physical and Engineering Sciences,*, 358:2811–2845.

National Transportation Safety Board (2017). Marine accident report: Capsizing and sinking of fishing vessel destination. *U.S. Coast Guard*.

National Transportation Safety Board (2021). Marine accident report: Capsizing and sinking of commercial fishing vessel scandies rose. *U.S. Coast Guard*.

Ryerson, C. (1995). Superstructure spray and ice accretion on a large US Coast Guard Cutter. *J. Atmospheric Research*, 36:321–337.

Ryerson, C. (2009). Assessment of superstructure ice protection as applied to offshore oil operations safety. *US Army Cold Regions Research and Engineering Laboratory, Report 09-4*.

Stallabrass, J. (1980). Trawler icing. a compilation of work done at the national research center. *Mechanical Engineering Report MD-56, N.R.C. No. 19372*.

Zakrzewski, W. (1986). Icing of fishing vessels, part i: Splashing a ship with spray. 8th *International Association for Hydro-environment Engineering and Research on Ice*.

Zarling, J. (1980). Heat and mass transfer from freely falling drops at low temperatures. *US Army Cold Regions Research and Engineering Laboratory, Report B0-1B*.